https://doi.org/10.5194/egusphere-2026-3001
Preprint. Discussion started: 3 July 2026

Correction of Diurnal Errors in Dielectric-Based In-Situ Soil Moisture Measurements via a Stacked LSTM Framework

Eunkyo Seo[1,2], Seongjun Bae[1], Junnyeong Han[1], Cheolhee Yoo[3,4], Paul A. Dirmeyer[2]

[1] Department of Environmental Atmospheric Sciences, Pukyong National University, Busan, 48513, Republic of Korea
[2] Center for Ocean-Land-Atmosphere Studies, George Mason University, Fairfax, Virginia, 22030, United States
[3] Jet Propulsion Laboratory, California Institute of Technology, Pasadena, CA 91109, United States
[4] Major in Smart City, Pusan National University, Busan, 46241, Republic of Korea

Correspondence to: Eunkyo Seo (eseo@pknu.ac.kr)

Abstract. Soil moisture (SM) is a fundamental variable in land-atmosphere interactions, yet in-situ measurements from dielectric-based sensors often suffer from systematic temperature sensitivity known as the Maxwell-Wagner polarization effect. This sensitivity induces spurious daytime peaks that contradict the physical reality of evapotranspiration-driven daytime dry-down. In this study, we propose a data-driven approach using stacked Long Short-Term Memory (LSTM) networks to correct these temperature-induced diurnal errors in the International Soil Moisture Network (ISMN) by integrating in-situ observations with physically constrained diurnal patterns from ERA5-Land and MERRA-2 reanalysis datasets.

The LSTM-based correction ($ISMN_{LSTM}$) effectively reverses the spurious positive correlations between diurnal cycles of SM and soil temperature to physically consistent negative correlations, demonstrating superior robustness across various sensor technologies compared to a recent reanalysis-informed Fourier filtering method that can struggle with regional biases. Performance evaluations reveal a significant enhancement in diurnal temporal correlation, with $ISMN_{LSTM}$ achieving R=0.89 against reference observations compared to the raw ISMN (R=0.14). Gradient-based sensitivity analysis confirms that the model's predictive logic is rooted in physical processes, with short-lag (1–3 hours) thermal forcing from high-frequency components and broadly distributed sensitivity to low-frequency components representing background land surface state, reflecting a multi-scale information integration. Furthermore, the diurnally adjusted SM in flux tower observations reveals physically realistic land-atmosphere coupling with negative SM-latent heat flux correlations throughout the diurnal cycle, which are fundamentally misdiagnosed as weakly positive in the original observations. Overall, the LSTM-based correction framework provides a reliable foundation for the initialization of numerical weather prediction models, the validation of sub-daily satellite SM retrievals, and advancing the understanding of sub-daily land-atmosphere interactions.

https://doi.org/10.5194/egusphere-2026-3001
Preprint. Discussion started: 3 July 2026

1 Introduction

Soil moisture (SM), designated as an essential climate variable by the World Meteorological Organization (WMO), is a key component of the water, energy, and carbon cycles within land surface processes. By regulating the exchanges of water and energy between the land surface and the atmosphere, SM plays a central role in land–atmosphere interactions. Through its control of evapotranspiration (ET) and boundary-layer dynamics, SM influences precipitation, surface energy partitioning, and the diurnal variations of near-surface temperature, humidity, and latent (LH) and sensible (SH) heat fluxes (Santanello et al., 2018; Seneviratne et al., 2010).

Land–atmosphere interactions can be broadly categorized into two regimes separated by a critical SM threshold (see Fig. 2 in Seo et al., 2024). On the wet side of this threshold, the surface lies in an energy-limited regime where the available atmospheric energy primarily governs surface fluxes, whereas on the dry side, the surface enters a water-limited regime in which the partitioning of available energy into LH and SH is strongly controlled by the amount of SM available for evaporation (Seo et al., 2019; Dong et al., 2022). The water-limited regime includes a transitional phase, characterized by a gradual decline in LH as SM decreases, and a dry phase, which occurs beyond the critical breakpoint where evaporation is nearly absent. In this dry regime, the lack of evaporative cooling leads to hypersensitive responses of surface temperature to SM variability, representing one of the key physical mechanisms that amplify the occurrence and intensity of heatwaves (Seo et al., 2020; Tak et al., 2024; Hsu et al., 2024).

While this energy-limited and water-limited framework has been widely applied at daily to seasonal timescales, the same physical processes operate distinctly within the diurnal cycle. Under precipitation-free conditions, near-surface SM typically reaches its maximum around dawn, when ET is minimal and hydraulic lift by plant roots facilitates the nocturnal transport of water from deeper, moister soil layers to the drier surface layer, partially replenishing surface soil water (Richards and Caldwell, 1987). As incoming solar radiation intensifies after sunrise, ET increases rapidly, drawing water from the near-surface soil layer and driving SM to its daily minimum in the late afternoon (Seo and Dirmeyer, 2022). Consequently, the diurnal SM cycle reflects the integrated response of surface energy partitioning, stomatal regulation, and soil hydraulic processes, and any spurious disruption of this cycle, such as temperature-induced sensor artifacts, directly obscures the physical reality of near-surface water and energy exchanges.

SM also modulates precipitation through bidirectional coupling processes (Sun et al., 2025; Ek and Holtslag, 2004; Findell and Eltahir, 2003; Ferguson and Wood, 2011). Within the diurnal cycle, the morning SM state plays a particularly critical role in determining the subsequent afternoon convective activity. Wetter SM in the early morning enhances ET during the morning hours, supplying moisture and latent energy to the atmospheric boundary layer. This moistening and destabilization of the boundary layer during the morning hours primes the atmosphere for convective initiation in the afternoon (Findell and Eltahir, 2003). In semi-arid regions, afternoon rainfall tends to occur preferentially over relatively drier soils, where enhanced sensible heating and mesoscale circulations trigger convective initiation, a mechanism known as negative SM–precipitation feedback (Taylor et al., 2012). In contrast, positive SM–precipitation coupling dominates in humid regions, where higher morning SM

https://doi.org/10.5194/egusphere-2026-3001
Preprint. Discussion started: 3 July 2026

enhances ET throughout the day, maintaining boundary-layer humidity and thereby increasing the likelihood of subsequent precipitation (Wei and Dirmeyer, 2012; Moon et al., 2019; Hay-Chapman and Dirmeyer, 2023). These diurnal-scale coupling processes highlight that accurate representation of the morning SM state is essential for understanding how land surface conditions cascade into afternoon convective development, underscoring the need for physically consistent sub-daily SM observations.

To better understand the spatiotemporal variability of SM and its role in land–atmosphere interactions, in-situ observations remain indispensable. In-situ SM measurements are obtained using various sensing techniques, including capacitance and frequency-domain reflectometry (FDR) sensors that estimate soil dielectric permittivity, time-domain reflectometry (TDR) probes that determine the travel time of electromagnetic pulses along waveguides, and neutron- or cosmic-ray-based sensors that infer soil water content from the moderation of high-energy neutrons generated by cosmic rays in the atmosphere. These techniques provide complementary information across different spatial scales, ranging from point-scale sensors capturing fine-scale soil heterogeneity to area-integrated observations representing footprints of several hectares. The International Soil Moisture Network (ISMN; Dorigo et al., 2021) compiles such in-situ SM measurements from numerous regional networks worldwide and harmonizes them using standardized data formats and rigorous quality control procedures to ensure consistency and comparability. Likewise, the COSMOS-UK project (Zreda et al., 2012), operated by the UK Centre for Ecology & Hydrology, provides continuous SM observations using the cosmic-ray neutron sensing (CRNS) technique, which enables non-invasive observations over footprints of hundreds of meters. These coordinated SM monitoring systems provide an essential empirical foundation for investigating SM dynamics, validating land-surface parameterizations, and advancing process-based understanding of land–atmosphere coupling.

Although relatively popular, dielectric-based SM sensors exhibit substantial temperature sensitivity due to the Maxwell–Wagner polarization effect (Chelidze and Gueguen, 1999; Chen and Or, 2006b). This phenomenon arises at the interfaces of soil constituents, namely air, water, and mineral particles, where contrasts in dielectric permittivity and electrical conductivity cause interfacial polarization (Chen and Or, 2006a). As temperature increases, enhanced ion mobility and charge relaxation alter the bulk dielectric response measured by the sensor, leading to temperature-dependent artifacts in SM estimates (Mittelbach et al., 2012; Ojo et al., 2015). These effects are particularly pronounced in low-frequency sensors such as capacitance, impedance, and frequency-domain reflectometry (FDR) probes, which are widely used owing to their low cost and operational simplicity (Francesca et al., 2010; Mane et al., 2024). Consequently, in the absence of frequent precipitation, these sensors often display spurious daytime SM peaks that are positively correlated with soil temperature (TS), even though the physical reality dictated by the surface water balance is a daytime minimum due to ET-driven drying, especially in shallow soils (Han et al., 2026). Such unrealistic diurnal behavior introduces artificial water imbalances and hinders accurate interpretation of sub-daily land–atmosphere processes (Seo and Dirmeyer, 2022).

To mitigate these sensor-induced biases, mechanistic approaches model the temperature dependence of dielectric permittivity based on its frequency response or employ laboratory calibration and energy balance modeling to remove thermal biases, while empirical approaches estimate correction coefficients from observed diurnal co-variations of temperature and

https://doi.org/10.5194/egusphere-2026-3001
Preprint. Discussion started: 3 July 2026

permittivity (Chanzy et al., 2012; Kapilaratne and Lu, 2017). More recently, a comprehensive Fourier transform-based diurnal adjustment approach using physically constrained land surface model datasets has been shown to improve diurnal SM behavior, capturing morning peaks and afternoon minima consistent with ET and energy-limited surface processes (Han et al., 2026). However, these approaches often rely on auxiliary reanalysis data or site-specific calibration, which can limit their scalability across diverse sensor networks, particularly when reanalysis products exhibit regional biases.

While deep learning techniques have been increasingly adopted for predicting SM variability at daily or longer timescales (O and Orth, 2021; Wang et al., 2024), their potential for correcting sub-daily diurnal errors remains largely underexplored. Given that in-situ diurnal observations provide a sufficiently large number of training samples even from relatively short observational records, deep learning frameworks are particularly well-suited for capturing the complex temporal dynamics of the diurnal SM cycle. In particular, the high-frequency nature of global in-situ networks yields an ample volume of diurnal cycle samples, including periods in which sensors exhibit minimal temperature sensitivity. These periods can serve as reliable 'true' signals for model training, allowing the network to internalize the underlying physical relationships between SM and its driving variables. Once developed, such a deep learning-based framework offers a scalable and operationally efficient solution that can be deployed across observation sites to mitigate sensor artifacts in real time, providing global applicability at the inference stage without further reliance on auxiliary reanalysis datasets.

In this study, we aim to correct the diurnal error of in-situ SM observations by applying a data-driven correction approach based on Long Short-Term Memory (LSTM) networks, a type of recurrent neural network designed to capture temporal dependencies in sequential data. LSTM networks are particularly effective for learning the lagged thermal response of soil dielectric properties (Kratzert et al., 2018). Unlike traditional physically based correction methods, the LSTM approach directly learns the nonlinear relationships between SM, TS, and other variables relevant to the diurnal SM evolution from in-situ observations and physically constrained reanalysis products. This data-driven framework is designed to bridge the gap between flexibility and physical consistency. By training on physically consistent diurnal cycles, we evaluate whether the LSTM can robustly eliminate spurious daytime peaks and recover the ET-driven afternoon drawdown, and we benchmark its performance against the established Fourier transform-based method (Han et al., 2026). The proposed framework is expected to offer a scalable correction solution applicable to diverse sensing techniques, supporting improved characterization of sub-daily land–atmosphere interactions and the validation of sub-daily satellite SM retrievals.

2 Data

2.1 In-situ observations

To overcome the challenges posed by the fragmented and inconsistent formats of in-situ SM observations, the International Soil Moisture Network (ISMN; Dorigo et al., 2021) was established as a centralized, standardized repository. By implementing rigorous quality control and harmonization protocols, the ISMN effectively integrates diverse monitoring data into a unified

https://doi.org/10.5194/egusphere-2026-3001
Preprint. Discussion started: 3 July 2026

system. It currently hosts data from more than 2,900 sites across 77 networks worldwide. While ISMN provides SM and soil temperature (TS) observations at various depths, various measurement sensors are used at each station, even for the same variable. For instance, SM data comes from a diverse set of sensors, such as electromagnetic techniques (e.g., TDR, TDT, FDR, capacitance, and impedance) and cosmic-ray neutron sensing. Most observations have an hourly temporal resolution with a consistent format and units convention. The ISMN dataset has been widely used to investigate the complexities of soil physics and validate satellite-based and modeled SM products.

We utilize ISMN SM and TS measurements at depths within the top 10 cm of soil, most susceptible to temperature sensitivity. The dataset is filtered to include only "good" quality flags with complete 24-hour records to ensure an accurate representation of the entire diurnal cycle. To ensure a sufficient number of diurnal samples for robust analysis, only stations with a minimum of 92 days of overlapping SM and TS data are selected. To account for the temperature sensitivity of dielectric-based sensors, which can induce spurious positive temporal correlations between the diurnal cycles of SM and TS (Fig. 1), we identified reference sites based on sensor physics. Consistent with Han et al. (2026), we designate 100 stations, comprising 10 non-dielectric-based cosmic-ray sensors and 90 high-frequency dielectric sensors (e.g., TDR and TDT), as reference sites ($ISMN_{ref}$), as they exhibit the physically expected negative SM-TS correlation. The reference observations are excluded from the LSTM-based correction.

2.2 Land Reanalysis Datasets

ERA5-Land (Muñoz-Sabater et al., 2021) is a global reanalysis dataset that provides hourly land surface variables at an enhanced spatial resolution of 9 km (0.1°), compared to the 31 km resolution of the standard ERA5. It operates as an offline simulation using the Carbon Hydrology-Tiled ECMWF Scheme for Surface Exchanges over Land (CHTESSEL) land surface model, driven solely by ERA5 atmospheric forcing. To improve the representation of near-surface states, ERA5-Land incorporates topographic adjustments, such as correcting air temperature via a lapse rate and recalculating surface pressure and humidity accordingly. Furthermore, it features updated physical parameterizations, including revised soil thermal conductivity under frozen conditions and improved soil water balance closure. These enhancements allow ERA5-Land to yield superior performance in reproducing SM time series when validated against global in-situ measurements (Beck et al., 2021).

MERRA-2 (Gelaro et al., 2017) is a global reanalysis produced by NASA's Global Modeling and Assimilation Office (GMAO) using the Goddard Earth Observing System version 5 (GEOS-5) atmospheric data assimilation system with a 3D-Var analysis scheme. A distinctive feature of MERRA-2 is its use of the Catchment LSM, which realistically captures hillslope hydrology by partitioning each grid cell into distinct saturated, unsaturated, and wilting regions (Koster et al., 2000). For the land surface component, precipitation is corrected using satellite- and gauge-based datasets, yielding a more accurate representation of the land hydrological cycle. For this study, we utilized hourly SM estimates for the surface layer (0–5 cm) at a spatial resolution of 0.625° × 0.5°, taking advantage of its robust treatment of sub-grid scale topographical influences and runoff processes.

https://doi.org/10.5194/egusphere-2026-3001
Preprint. Discussion started: 3 July 2026

In this study, hourly SM and TS from both reanalysis datasets are utilized to constrain the diurnal cycle of in-situ measurements, using the surface layer (0–7 cm for ERA5-Land and 0–5 cm for MERRA-2). These variables are selected for their physically constrained behavior driven by land surface water and energy balance processes.

2.3 Flux tower observations

To investigate the influence of the diurnal SM correction on L-A interactions, flux tower observations are employed to analyze the relationship between SM and LH at sub-daily timescales. In flux tower observations, land surface heat fluxes are measured using the eddy covariance method, whereas SM is measured using dielectric-based sensors (e.g., TDR, FDR). These sensors are subject to the same temperature-induced diurnal errors described previously.

This study utilizes three flux tower datasets: FLUXNET2015 (Pastorello et al., 2020), AmeriFlux (Novick et al., 2018), and the Integrated Carbon Observation System (ICOS; Heiskanen et al., 2022), covering observations spanning approximately the past 30 years. Where FLUXNET2015 spatially and temporally overlaps with AmeriFlux and ICOS data, FLUXNET2015 is given priority, with the other datasets used to extend its temporal coverage. SM measurements at depths up to 10 cm are utilized to ensure consistency across all sites. Among stations with both SM and LH observations, 178 stations with at least 92 days of complete 24-hour records are selected in this study, following the same data gathering strategy as in Han et al. (2026). The analysis is conducted at the diurnal timescale using hourly records during the hemispheric warm season (MJJAS for the Northern Hemisphere and NDJFM for the Southern Hemisphere), as L-A interactions driven by solar radiation are most prominent during this period. The flux tower sites are predominantly located in mid-latitude regions, where vegetated environments typically represent energy-limited regimes in which sufficient daytime energy availability enhances ET, subsequently leading to SM depletion.

3 Methodology

3.1 Construction of LSTM Model

To mitigate temporal errors in in-situ SM observations, particularly within the diurnal cycle, this study develops a deep learning framework based on Long Short-Term Memory (LSTM) networks (Hochreiter and Schmidhuber, 1997). The LSTM architecture was chosen for its ability to capture long-term temporal dependencies in time-series data while addressing the vanishing gradient problem inherent in standard Recurrent Neural Networks (RNN). By maintaining a specialized cell state that carries information across time steps, the model effectively learns the complex, time-lagged coupling between SM and its meteorological forcing variables.

The overall modeling workflow, illustrated in Figure 2, consists of three sequential stages: (i) data preprocessing, in which input variables from in-situ observations and reanalysis products are decomposed into low- and high-frequency components

https://doi.org/10.5194/egusphere-2026-3001
Preprint. Discussion started: 3 July 2026

and filtered to retain physically consistent diurnal cycles for training; (ii) model building and training, in which a stacked LSTM network augmented with a Physics Constraint Layer is trained to predict the high-frequency component of ISMN SM; and (iii) independent evaluation, in which the trained model is applied to $ISMN_{ref}$ excluded from training to assess performance through temporal correlation analysis and gradient-based sensitivity diagnostics. Each stage is described in detail below.

3.1.1 Data preprocessing

The input dataset (X_t) for the LSTM model is constructed from multiple sources, integrating in-situ observations with high-resolution reanalysis products. A selective approach is applied to the input variables: for the ISMN, only the TS variable is utilized to avoid target leakage, since ISMN SM itself serves as the modeling target. For the ERA5-Land and MERRA-2 datasets, a broader suite of variables including SM, TS, and LH is incorporated. LH is included because, in the absence of precipitation, it represents the dominant sink term governing the temporal tendency of SM in the water balance equation. TS provides information on the diurnal cycle of incoming surface energy that drives ET.

Prior to frequency decomposition, each time series is screened to exclude precipitation-affected periods, which can mask the subtle diurnal signals driven by evaporative demand through rapid post-precipitation dry drifting. For ISMN sites, rainy days are identified when the daily SM tendency exceeds +0.5 standard deviations, an optimized threshold based on sensitivity tests against collocated precipitation data (Han et al., 2026). For the LSMs, rainy days are filtered using their precipitation outputs with a threshold of 0.1 mm daily total.

A frequency separation procedure is then applied to each variable: a 24-hour centered moving average is computed as the low-frequency (LF) component and subtracted from the original hourly time series to obtain the high-frequency (HF) component. This decomposition yields a total of 14 input features (2 from ISMN: TS, 6 from ERA5-Land: SM, TS, LH, and 6 from MERRA-2: SM, TS, LH). The modeling target (Y_t) is defined as the HF component of ISMN SM.

To ensure that the network learns physically realistic diurnal dynamics, a training-only filter is applied to the target (highlighted in orange in Fig. 2): only diurnal cycles dominated by evaporative demand are retained for training, identified by a temporal correlation between SM and TS (R(SM,TS)) below -0.34 over 24-hour windows, corresponding to a statistically significant negative correlation ($p < 0.1$). This physically motivated selection yields a curated training dataset of 159,631 diurnal samples. Importantly, this filter is applied only during training; at inference, the trained model is applied to the full HF time series regardless of R(SM,TS). All curated input variables are then scaled using min-max normalization, and an 18-hour sliding window is applied to generate sequential input samples ($X_{t-17}, X_{t-16}, \dots, X_t$).

3.1.2 LSTM model architecture for SM diurnal error correction

The total preprocessed dataset is partitioned into training (70%) and validation (30%) subsets, both drawn from non-reference ISMN stations. The validation set is used for early stopping: training is terminated if the validation loss fails to improve for 30 consecutive epochs, and the final model weights are selected at the point of minimum validation loss to prevent overfitting.

https://doi.org/10.5194/egusphere-2026-3001
Preprint. Discussion started: 3 July 2026

The proposed model utilizes a stacked LSTM architecture consisting of three hidden layers, each with 256 units. The input data of shape (batch size, sequence length, number of input features) is fed into the first LSTM layer, which learns both short- and long-term temporal dependencies through its internal gate operations, producing a hidden state (h_t) of shape (batch size, sequence length, 256). This hidden state is then passed to the subsequent LSTM layer after applying a dropout rate of 0.1 (Srivastava et al., 2014), retaining 90% of the connections. The second LSTM layer operates in the same manner, with dropout again applied before passing to the third LSTM layer. In the final LSTM layer, no dropout is applied, and the output is passed directly to the subsequent dense layers. Each LSTM cell (C_t) regulates information flow through three primary gating mechanisms: the forget, input, and output gates. The forget gate employs a sigmoid activation function to determine which historical information from the previous cell state should be discarded, while the input gate identifies new relevant information to be updated in the current cell state. The output gate subsequently controls the magnitude of the signal sent to the hidden state (h_t), which serves as the short-term memory for capturing temporal dependencies. Sigmoid functions are used to regulate the flow (0 to 1), and hyperbolic tangent functions scale the updates within a range of -1 to 1. The information extracted from the final LSTM sequence is processed through a sequence of dense layers consisting of two hidden layers with 128 and 64 units incorporating ReLU activation functions (Nair and Hinton, 2010), followed by a single output layer to generate the final prediction.

To enforce physical plausibility of the reconstructed SM time series, a Physics Constraint Layer is integrated between the final dense layer and the model output (Fig. 2). Since the training target is the HF component of SM (SM_HF), reconstructing the full SM time series requires adding back the LF component, which may yield non-physical negative SM values in dry regimes with pronounced diurnal amplitudes. The Physics Constraint Layer addresses this issue through a five-step procedure: (1) the predicted normalized SM_HF from the linear output layer is denormalized to physical units (m^3/m^3) using the min-max parameters from the training set; (2) the ISMN low-frequency component (SM_LF) is added to reconstruct the total SM time series; (3) a ReLU activation is applied to the total SM, enforcing the physical constraint SM ≥ 0 by clipping non-physical negative values to zero while leaving non-negative values unchanged; (4) SM_LF is subtracted back to recover the HF component; and (5) the resulting HF series is re-normalized to produce the final output (Y_t). Crucially, this layer is embedded within the training loop rather than applied as post-processing. As gradients propagate through the ReLU operation during backpropagation, the network is penalized whenever its predictions would result in negative reconstructed SM, and the model therefore internalizes the physical lower bound as an implicit training constraint. This design eliminates the need for external post-processing corrections such as the Standard Normal Deviate Scaling (SNDS) employed in the Fourier-based approach (Han et al., 2026) to prevent non-physical negative SM values.

The model is implemented in PyTorch and optimized using the Adam optimizer (Kingma and Ba, 2014) with a learning rate of 0.0006 and a Mean Squared Error (MSE) loss function computed on the normalized SM_HF domain (i.e., the output Y_t of the Physics Constraint Layer compared to the normalized target). Training is performed with a batch size of 32, which has been shown to balance computational efficiency and generalization performance in deep learning tasks (Masters and Luschi, 2018).

https://doi.org/10.5194/egusphere-2026-3001
Preprint. Discussion started: 3 July 2026

3.1.3 Independent evaluation

For unbiased performance evaluation, the trained model is applied to the $ISMN_{ref}$, which is excluded from both training and validation. The corrected outputs, hereafter referred to as $ISMN_{LSTM}$, are evaluated against the reference observations through temporal correlation analysis at the diurnal scale. To validate the efficacy of this approach, the performance of $ISMN_{LSTM}$ is further benchmarked against the Fourier-based time-filtered SM data ($ISMN_{FFT}$) introduced by Han et al. (2026) as well as the original ISMN observations. In addition, gradient-based sensitivity analysis is conducted to interpret the physical basis of the model's predictions (Section 3.2).

3.2 Interpretation of model physics: Gradient-based lag-dependent sensitivity

Deep learning models, particularly multi-layered LSTMs, are often characterized as "black-box" systems due to their complex internal architectures and high-dimensional parameter spaces. To ensure that the corrections provided by the introduced LSTM model are rooted in physical processes rather than mere statistical artifacts, we conducted a gradient-based sensitivity analysis (Simonyan et al., 2013) to interpret the model's internal decision-making and quantify the temporal coupling between SM and model input variables. This approach allows for a diagnostic evaluation of how the model utilizes historical information at specific time lags to predict the current SM state.

The mathematical foundation of this interpretation lies in calculating the partial derivative of the model output (Y_t) with respect to the input vector (X_t) at each time step (τ) within the 18-hour sliding window. However, because the model input variables possess their physical units and widely varying scales, their raw gradients ($\partial Y_t / \partial X_{i,t-\tau}$) are not directly comparable. To overcome this limitation and enable a robust comparison of relative sensitivity, we calculated the standardized sensitivity ($S_{i,\tau}$) by multiplying the absolute gradient of each feature by its corresponding long-term standard deviation (σ_i) derived from the training dataset:

$$S_{i,\tau} = \frac{1}{N}\sum_{j=1}^{N}\left|\frac{\partial Y_t^j}{\partial X_{i,t-\tau}^j}\right| \times \sigma_X \qquad (1)$$

where i represents the specific input variable, $\tau \in [0,17]$ denotes the time lag in hours, and N denotes the total number of randomly selected samples utilized for the model evaluation. We fix $N = 320{,}506$, indicating the entirety of diurnal samples from reference sites ($ISMN_{ref}$), to ensure statistical robustness. This multiplication effectively rescales the sensitivity, representing the expected change in the output soil moisture for a one-standard-deviation change in the input variable. This transformation is crucial for identifying which physical driver exerts the dominant influence on the diurnal SM.

The sensitivity calculation is implemented using the automatic differentiation (autograd) engine of the PyTorch framework, which enables the precise backpropagation of gradients from the final prediction layer through the hidden states of the stacked LSTM. Since the final prediction Y_t is a recursive function of the hidden state (h_t), these gradients capture the cumulative "weight" assigned to each hour by the model's forget, input, and output gates. By analyzing the peak values and temporal decay

https://doi.org/10.5194/egusphere-2026-3001
Preprint. Discussion started: 3 July 2026

patterns of these standardized sensitivities, we can physically validate the characteristic response time of SM to atmospheric heating and evaporation cycles. This interpretability framework confirms whether the LSTM has successfully internalized the time-lagged physical dependencies that characterize the land-surface system.

3.3 Land coupling strength

To investigate the land-atmosphere (L-A) coupling between SM and LH in diurnal time scale, we employ a correlation term of the Terrestrial Coupling Index (TCI; Dirmeyer, 2011; Seo and Dirmeyer, 2022) which quantifies the statistical association between a source variable (SV) and a target variable (TV). TCI incorporates both the sensitivity of the target variable to variability in the source variable and the magnitude of variability in the target variable. TCI is formulated as:

$$TCI(SV, TV) = R(SV, TV) \times \sigma(TV) \quad (2)$$

where R and σ represents the temporal correlation coefficient and the standard deviation, respectively. It should be noted that TCI does not imply causality and should be interpreted as a measure of statistical association only. In this study, SM and LH are set as the source and target variables, respectively. When LH is the target, positive or negative TCI values indicate that the L-A coupling chain is primarily triggered by SM or net radiation, respectively, corresponding to water- or energy-limited regimes (see Fig. 2 in Seo et al., 2024). Compared with conventional applications using daily to monthly data, land coupling within the diurnal cycle is primarily explained by the relationship between SM and LH, because LH variability strongly depends on the incoming energy at the surface. Therefore, this study adopts $R(SV, TV)$ to measure the strength of land coupling and the direction of land–atmosphere interactions. Hourly time series are reconstructed by averaging the values from multiple days at each hour, following the removal of low-frequency variability using a 24-hour centered moving average.

4 Results

4.1 Improvement in the physical representation of constrained SM diurnal variations

The comparative analysis of the temporal correlation between diurnal SM and TS highlights the performance of the LSTM-based diurnal correction. The uncorrected ISMN data exhibits physically spurious positive correlations, particularly during the boreal summer season and at sites characterized by relatively dry SM climatology (Fig. 1). This phenomenon contradicts the physical coupling where rising temperatures drive increased evaporative demand, which should result in a depletion of surface SM and a corresponding negative correlation. These spurious patterns are likely artifacts of the thermal sensitivity of the measurement sensors, which often causes SM readings to fluctuate in phase with diurnal temperature cycles. In contrast, the $ISMN_{LSTM}$ dataset demonstrates a comprehensive shift toward physically consistent negative correlations across nearly all stations and seasons (Fig. 3). The timely corrected result indicates that the LSTM-based model successfully learns the inverse relationship between SM and TS. Specifically, in dry sites during the boreal summer, where the ISMN data shows the strong

https://doi.org/10.5194/egusphere-2026-3001
Preprint. Discussion started: 3 July 2026

spurious signals, the LSTM correction effectively reverses the correlation sign. This indicates that the model's gating mechanisms effectively filtered out the non-physical noise while retaining the diurnal dry-down signals driven by evaporation.

To evaluate the reliability of the diurnal correction across diverse measurement approaches, the temporal correlations between diurnal SM and TS are analyzed for six different sensor types (Fig. 4). In the raw ISMN observations, common sensor types such as Impedance, Capacitance, and Frequency Domain Reflectometry (FDR) exhibit dominant spurious positive correlations (Fig. 4a). The result from $ISMN_{FFT}$ shows a partial improvement in physical consistency for most sensors, yet its performance is notably inconsistent across different measurement technologies (Fig. 4b). Specifically, while the correlations for Impedance and Capacitance sensors are shifted to -0.72 and -0.75, respectively, the improvement for FDR sensors remained limited, reaching a median value of -0.22. This lack of performance for FDR sensors in the FFT-based time correction is primarily attributed to the inherent biases and poor simulation performance of the reanalysis products (e.g., ERA5-Land and MERRA-2) at those specific station locations, which are utilized as the reference for frequency separation.

In contrast, the $ISMN_{LSTM}$ demonstrates remarkable robustness and consistency (Fig. 4c), successfully producing realistic negative correlations regardless of the sensor type or the quality of the underlying reanalysis data. For the FDR sensors, the LSTM correction achieved a high negative correlation of -0.57, significantly outperforming the $ISMN_{FFT}$. This indicates that the stacked LSTM architecture does not merely rely on the reanalysis data's performance but effectively extracts and utilizes the physical temporal patterns between SM and TS anomalies.

4.2 Evaluation of reconstructed diurnal SM dynamics and model interpretation

To assess the efficacy of the proposed LSTM-based correction in recovering realistic SM dynamics, measured by impedance sensor, we evaluate the performance of the corrected datasets at diurnal temporal scales (Fig. 5). The original ISMN time series (R=-0.62) exhibits a strong negative correlation with the reference, indicating a pronounced diurnal error characterized by an anomalous daytime increase in SM, which is physically inconsistent with the expected evapotranspiration-driven drying during peak solar radiation hours. The $ISMN_{FFT}$ (R=0.34) partially mitigates this systematic error, yielding a positive but modest correlation with the reference. In contrast, the $ISMN_{LSTM}$ (R=0.66) demonstrates a substantially improved agreement with the reference at this specific site, effectively capturing the daytime drying phase while suppressing the spurious diurnal fluctuations present in the original ISMN data. These results suggest that the proposed LSTM-based correction framework outperforms the Fourier-based approach in reconstructing physically consistent diurnal SM dynamics.

Figure 6a presents the composite diurnal cycles of SM anomalies across 16 stations, comparing the ISMN, $ISMN_{FFT}$, and $ISMN_{LSTM}$ against the $ISMN_{ref}$. The ISMN observations exhibit a distinct non-physical phase, with SM increasing during the morning time (06:00–12:00 LST), peaking in synchronization with solar heating. This behavior contradicts the expected physical dry-down driven by evaporative demand. In contrast, the $ISMN_{LSTM}$ results demonstrate a significant improvement in capturing the diurnal phase, closely following the $ISMN_{ref}$ benchmark. The LSTM correction effectively reconstructs the daytime SM depletion, maintaining a consistent downward trend during the hours of peak temperature and LH, thereby aligning

https://doi.org/10.5194/egusphere-2026-3001
Preprint. Discussion started: 3 July 2026

with the physical constraints of the land-surface system. The robustness of the LSTM approach is further highlighted by its performance in diurnal temporal resolutions (Fig. 6b). At the hourly scale, the $ISMN_{LSTM}$ achieves a temporal correlation of 0.89 across 16 stations, representing a substantial improvement over the raw ISMN (R=0.14) and the $ISMN_{FFT}$ (R=0.66). This hourly enhancement is critical for applications requiring temporally high-resolution data, such as the validation of satellite-derived SM or the initialization of numerical weather prediction models.

To elucidate the predictive logic of the trained LSTM and verify its physical consistency, a gradient-based lag-dependent sensitivity analysis is conducted (Fig. 7), which evaluates how strongly the predicted SM responds to each input variable at preceding time steps within the 18-hour sliding window, as detailed in Section 3.2. A large sensitivity value at a short lag indicates that the model relies heavily on the recent state of that variable, whereas sensitivity at longer lags reflects the use of information from further back in time. This approach quantifies how the predicted SM responds to variations in input variables ($X_{i,t-\tau}$) across the preceding 18-hour sequence (τ), providing a temporal map of the model-learned response time of land surface processes.

Among the HF inputs, the high-frequency components of TS and SM (TS_HF, SM_HF) from ERA5-Land exhibit the strongest sensitivities, concentrated within short lead times of 1–3 hours, followed by ISMN TS_HF and MERRA-2 TS_HF over a similar lag window. This concentration of gradient magnitude near the prediction time indicates that recent diurnal thermal forcing and background SM dynamics from reanalysis are the primary drivers used by the model to adjust the spurious phase shifts in the original SM observations. In contrast, the HF components of LH (LH_HF) from both reanalyses, as well as MERRA-2 SM_HF show negligible sensitivity, suggesting that LH_HF variability contributes little to the diurnal correction.

Although LF inputs are often assumed to provide only background context, LF variables exhibit pronounced and broadly distributed sensitivities across the lag window. The LF component of TS (TS_LF) from ERA5-Land shows particularly strong sensitivity over lead times of 3–7 hours, while the LF component of SM (SM_LF) from MERRA-2 maintains substantial sensitivity across nearly the entire 18-hour window. The LF component of LH (LH_LF) from ERA5-Land additionally exhibits a sensitivity peak at the shortest lead times (1–2 hours), consistent with the role of LH as the dominant sink term in the surface SM water balance during precipitation-free periods, as motivated by the input variable selection (Section 3.1). These patterns demonstrate that the model leverages the background land surface state, rather than relying solely on instantaneous thermal forcing, to constrain the amplitude and baseline of the predicted diurnal cycle.

Together, the HF and LF sensitivity patterns reveal a clear division of roles: HF inputs predominantly inform the short-term phase adjustment of the diurnal cycle, while LF inputs constrain the longer-term hydrological context within which the diurnal variability evolves. Notably, ERA5-Land contributes most strongly through its TS information at both frequency bands and through its high-frequency SM, whereas MERRA-2 provides complementary information primarily through its low-frequency SM dynamics. This complementarity supports the design choice of incorporating both reanalysis products as input, as each captures distinct aspects of the land surface system. The multi-scale (low- and high-frequency) and multi-source (ISMN, ERA5-Land, MERRA-2) architecture thereby enables the LSTM to perform corrections that are physically grounded in both immediate thermal forcing and background hydrological state.

https://doi.org/10.5194/egusphere-2026-3001
Preprint. Discussion started: 3 July 2026

4.3 Realization in land-atmosphere interactions

The distributions of TCI(SM, LH) and its components, R(SM, LH) and σ(LH), based on hourly data derived from the original flux tower observations (Fluxtower) and the diurnally adjusted datasets ($Fluxtower_{FFT}$ and $Fluxtower_{LSTM}$) are presented in Fig. 8 for the hemispheric warm season. Interpretation of this TCI is different than the conventional application using daily to monthly data: rather than quantifying subseasonal to interannual coupling between land and atmosphere, this analysis isolates coupling within the diurnal cycle (Dirmeyer et al., 2009). The R(SM, LH) shifts from 0.09 in the Fluxtower to -0.50 and -0.35 in $Fluxtower_{FFT}$ and $Fluxtower_{LSTM}$, respectively, indicating that diurnal adjustment substantially alters the diagnosed statistical relationship between SM and LH. These results highlight that the systematic diurnal errors in the original Fluxtower observations lead to a fundamental misdiagnosis of the L-A coupling regime, and that the LSTM-based correction provides a more physically consistent characterization of the land surface control on LH compared to the Fourier-based approach. Given that the LSTM-based approach demonstrates superior performance in correcting diurnal SM errors against ISMN reference sensors (Section 4.1), the more strongly negative R(SM, LH) values obtained from $Fluxtower_{FFT}$ suggest that the Fourier-based correction may overestimate the strength of energy-limited coupling processes. This potential overestimation likely arises from the strong dependence of the FFT-based method on reanalysis-derived diurnal patterns, which may not perfectly represent site-specific land surface conditions, thereby introducing a systematic bias in the diagnosed SM–LH relationship.

5 Summary and Conclusions

This study develops a novel data-driven framework based on a stacked LSTM network to correct temperature-induced errors in dielectric-based in-situ SM measurements. These systematic errors, primarily stemming from the Maxwell-Wagner polarization effect, have long hindered the physical realism of land surface water budgets by inducing spurious daytime peaks in phase with diurnal temperature fluctuations. By leveraging physically consistent diurnal patterns from high-resolution reanalysis datasets (ERA5-Land and MERRA-2), the proposed LSTM framework successfully restored realistic SM dynamics across a diverse global network of stations.

The results demonstrate that the $ISMN_{LSTM}$ effectively shifted the non-physical positive temporal correlations between the diurnal cycles of SM and TS to physically consistent negative correlations. This reversal is particularly pronounced in dry climate regimes and during the boreal summer, where sensor-induced artifacts are typically most severe, thereby accurately recovering the afternoon SM drawdown driven by evaporative demand. Furthermore, the model exhibited strong robustness across various sensor types, including Impedance, Capacitance, and FDR sensors. Unlike the Fourier-based filtering method ($ISMN_{FFT}$), which showed limited efficacy for FDR sensors with a correlation of -0.22 due to regional biases in reanalysis

https://doi.org/10.5194/egusphere-2026-3001
Preprint. Discussion started: 3 July 2026

products, the LSTM approach achieved a high negative correlation of -0.57 for FDR sensors, providing consistent and reliable corrections regardless of the measurement technology or the underlying quality of the reanalysis data.

By integrating both high-frequency (HF) and low-frequency (LF) features as input variables (e.g., surface soil moisture, soil temperature, and latent heat flux), the model significantly improves SM time series. The $ISMN_{LSTM}$ achieves a diurnal temporal correlation of 0.89 against reference observations, representing a substantial improvement over the raw ISMN (R=0.14) and the $ISMN_{FFT}$ (R=0.66), effectively capturing the daytime drying phase while suppressing the spurious diurnal fluctuations present in the original observations. The $ISMN_{LSTM}$ closely follows the reference diurnal cycle by effectively reconstructing the daytime SM depletion and maintaining a consistent downward trend during the hours of peak TS and LH, thereby aligning with the physical constraints of the land-surface system. The LSTM's predictive logic combines short-lag (1–3 hours) thermal forcing from the HF components of ERA5-Land TS and SM, with broadly distributed sensitivity to LF components that represent the background land surface state. This multi-scale information integration, supported by complementary contributions from ERA5-Land (TS-dominated) and MERRA-2 (SM-dominated), enables the model to correct both the phase and amplitude of the diurnal cycle in a physically consistent manner.

Compared with the Fourier-based filtering approach (Han et al., 2026), the LSTM framework offers significant methodological advantages. Notably, owing to the Physics Constraint Layer embedded within the training loop, it eliminates the need for auxiliary post-processing steps such as the diurnal mean correction used to align with nighttime baselines or the Standard Normal Deviate Scaling (SNDS) required to prevent non-physical negative soil moisture values. By learning the complex sequential dependencies of SM directly from the input variables, the LSTM framework maintains physical realism inherently without these manual adjustments. Furthermore, while the Fourier-based method specifically focuses on adjusting the diurnal frequency band, the LSTM model captures diurnal temporal dynamics and temporal dependencies within its recurrent architecture, thereby providing a more comprehensive correction of SM representations.

The implications of the diurnal correction extend beyond SM quality itself. The systematic diurnal errors present in the original flux tower observations are shown to fundamentally misdiagnose the L-A coupling regime, leading to a weakly positive R(SM, LH) that contradicts the physically expected energy-limited coupling during the warm season. Following diurnal adjustment, both the LSTM- and Fourier-based corrections reveal a shift toward negative R(SM, LH) values, reflecting a more physically consistent characterization of the SM-LH relationship. Notably, this sign reversal is primarily driven by changes in the statistical relationship between SM and LH. Furthermore, given that the LSTM-based approach demonstrates superior performance against ISMN reference sensors (Section 4.1), the more strongly negative R(SM, LH) values obtained from the Fourier-based correction suggest that this method may overestimate the energy-limited L-A coupling processes, likely arising from its strong dependence on reanalysis-derived diurnal patterns that may not perfectly represent site-specific land surface conditions.

This inherent methodological efficiency and robustness allow the LSTM framework to transcend site-specific constraints, enabling its widespread implementation across global in-situ networks that span diverse hydroclimatic regions, from arid to temperate zones. The scalability of the architecture facilitates the production of standardized, high-quality SM datasets across

https://doi.org/10.5194/egusphere-2026-3001
Preprint. Discussion started: 3 July 2026

the extensive ISMN, which are inherently corrected for sensor-induced thermal artifacts. A particularly notable aspect of this data-driven approach is its readiness for real-time applications. Since the LSTM model is already pre-trained on physically constrained dynamics, it can be seamlessly integrated into operational monitoring systems to provide instantaneous corrections for incoming in-situ observations. This capability for real-time data refinement is poised to enhance the accuracy of drought early-warning systems, improve the initialization of numerical weather prediction models, and support precision agricultural management. Furthermore, the $ISMN_{LSTM}$ dataset provides a robust foundation for the validation of sub-daily SM retrievals from polar-orbiting satellites and advances the understanding of sub-daily land-atmosphere interactions that have been previously hindered by observational limitations.

Acknowledgements

This research was supported by the National Research Foundation of Korea (NRF) grant funded by the Korea government (MSIT) (grant nos. RS-2026-25479797 and RS-2025-02363044).

Code availability

The source code used for the diurnal error correction through the LSTM framework is available at https://doi.org/10.5281/zenodo.19875807 (last access: 26 May 2026, Seo et al., 2026)

Data availability

In-situ observations from ISMN can be accessed and downloaded publicly via their website at https://ismn.earth/en/data/data-download/ (last access: 26 May 2026). Soil moisture and LH from flux tower observations can be accessed from the following websites: FLUXNET2015 at https://fluxnet.org/data/fluxnet2015-dataset/ (last access: 26 May 2026), AmeriFlux at https://ameriflux.lbl.gov/data/download-data/ (last access: 26 May 2026), and ICOS at https://www.icos-cp.eu/data-products (last access: 26 May 2026). Hourly data from the Copernicus Climate Change Service (C3S) ERA5-Land reanalysis are freely available through its online portal at https://cds.climate.copernicus.eu/datasets/reanalysis-era5-land?tab=overview (last access: 26 May 2026). The hourly MERRA-2 data are available for free through the NASA Goddard Earth Sciences (GES) Data and Information Service Center (DISC) at https://disc.gsfc.nasa.gov/datasets?project=MERRA-2 (last access: 26 May 2026).

https://doi.org/10.5194/egusphere-2026-3001
Preprint. Discussion started: 3 July 2026

Author contributions

Conceptualization: ES, SB, and PAD. Investigation, methodology, and formal analysis: ES, SB, JH, and CY. Writing (original draft preparation): ES. Writing (review and editing): SB, JH, CY, and PAD.

Competing interests

The contact author has declared that neither of the authors has any competing interests.

https://doi.org/10.5194/egusphere-2026-3001
Preprint. Discussion started: 3 July 2026

References

Beck, H. E., Pan, M., Miralles, D. G., Reichle, R. H., Dorigo, W. A., Hahn, S., Sheffield, J., Karthikeyan, L., Balsamo, G., and Parinussa, R. M.: Evaluation of 18 satellite-and model-based soil moisture products using in situ measurements from 826 sensors, Hydrology and Earth System Sciences, 25, 17-40, https://doi.org/10.5194/hess-25-17-2021, 2021.

Chanzy, A., Gaudu, J.-C., and Marloie, O.: Correcting the temperature influence on soil capacitance sensors using diurnal temperature and water content cycles, Sensors, 12, 9773-9790, https://doi.org/10.3390/s120709773, 2012.

Chelidze, T. and Gueguen, Y.: Electrical spectroscopy of porous rocks: a review—I. Theoretical models, Geophysical Journal International, 137, 1-15, https://doi.org/10.1046/j.1365-246x.1999.00799.x, 1999.

Chen, Y. and Or, D.: Geometrical factors and interfacial processes affecting complex dielectric permittivity of partially saturated porous media, Water resources research, 42, https://doi.org/10.1029/2005WR004744, 2006a.

Chen, Y. and Or, D.: Effects of Maxwell-Wagner polarization on soil complex dielectric permittivity under variable temperature and electrical conductivity, Water resources research, 42, https://doi.org/10.1029/2005WR004590, 2006b.

Dirmeyer, P. A.: The terrestrial segment of soil moisture–climate coupling, Geophysical Research Letters, 38, https://doi.org/10.1029/2011GL048268, 2011.

Dirmeyer, P. A., Schlosser, C. A., and Brubaker, K. L.: Precipitation, recycling, and land memory: An integrated analysis, Journal of Hydrometeorology, 10, 278-288, https://doi.org/10.1175/2008JHM1016.1, 2009.

Dong, J., Akbar, R., Short Gianotti, D. J., Feldman, A. F., Crow, W. T., and Entekhabi, D.: Can Surface Soil Moisture Information Identify Evapotranspiration Regime Transitions?, Geophysical Research Letters, 49, e2021GL097697, https://doi.org/10.1029/2021GL097697, 2022.

Dorigo, W., Himmelbauer, I., Aberer, D., Schremmer, L., Petrakovic, I., Zappa, L., Preimesberger, W., Xaver, A., Annor, F., and Ardö, J.: The International Soil Moisture Network: serving Earth system science for over a decade, Hydrology and Earth System Sciences, 25, 5749–5804, https://doi.org/10.5194/hess-25-5749-2021, 2021.

Ek, M. and Holtslag, A.: Influence of soil moisture on boundary layer cloud development, Journal of hydrometeorology, 5, 86-99, https://doi.org/10.1175/1525-7541(2004)005<0086:IOSMOB>2.0.CO;2, 2004.

Ferguson, C. R. and Wood, E. F.: Observed land–atmosphere coupling from satellite remote sensing and reanalysis, Journal of Hydrometeorology, 12, 1221-1254, https://doi.org/10.1175/2011JHM1380.1, 2011.

Findell, K. L. and Eltahir, E. A.: Atmospheric controls on soil moisture–boundary layer interactions. Part I: Framework development, Journal of Hydrometeorology, 4, 552-569, https://doi.org/10.1175/1525-7541(2003)004<0552:ACOSML>2.0.CO;2, 2003.

Francesca, V., Osvaldo, F., Stefano, P., and Paola, R. P.: Soil moisture measurements: Comparison of instrumentation performances, Journal of irrigation and drainage engineering, 136, 81-89, https://doi.org/10.1061/(ASCE)0733-9437(2010)136:2(81), 2010.

Gelaro, R., McCarty, W., Suárez, M. J., Todling, R., Molod, A., Takacs, L., Randles, C. A., Darmenov, A., Bosilovich, M. G., and Reichle, R.: The modern-era retrospective analysis for research and applications, version 2 (MERRA-2), Journal of Climate, 30, 5419-5454, https://doi.org/10.1175/JCLI-D-16-0758.1, 2017.

Han, J., Seo, E., and Dirmeyer, P. A.: Adjusting diurnal error in dielectric-based in situ soil moisture measurements via Fourier time-filtering using land surface model datasets, Hydrology and Earth System Sciences, 30, 2207-2223, https://doi.org/10.5194/hess-30-2207-2026, 2026.

Hay-Chapman, F. M. and Dirmeyer, P. A.: A Novel Method for Diagnosing Land–Atmosphere Coupling Sensitivity in a Single-Column Model, Journal of Hydrometeorology, 24, 2207-2223, https://doi.org/10.1175/JHM-D-22-0237.1, 2023.

Heiskanen, J., Brümmer, C., Buchmann, N., Calfapietra, C., Chen, H., Gielen, B., Gkritzalis, T., Hammer, S., Hartman, S., and Herbst, M.: The integrated carbon observation system in Europe, Bulletin of the American Meteorological Society, 103, E855-E872, https://doi.org/10.1175/BAMS-D-19-0364.1, 2022.

Hochreiter, S. and Schmidhuber, J.: Long short-term memory, Neural computation, 9, 1735-1780, https://doi.org/10.1162/neco.1997.9.8.1735, 1997.

Hsu, H., Dirmeyer, P. A., and Seo, E.: Exploring the mechanisms of the soil moisture-air temperature hypersensitive coupling regime, Water Resources Research, 60, e2023WR036490, https://doi.org/10.1029/2023WR036490, 2024.

Kapilaratne, R. J. and Lu, M.: Automated general temperature correction method for dielectric soil moisture sensors, Journal of Hydrology, 551, 203-216, https://doi.org/10.1016/j.jhydrol.2017.05.050, 2017.

Kingma, D. P. and Ba, J.: Adam: A method for stochastic optimization, arXiv preprint arXiv:1412.6980, https://doi.org/10.48550/arXiv.1412.6980, 2014.

Koster, R. D., Suarez, M. J., Ducharne, A., Stieglitz, M., and Kumar, P.: A catchment-based approach to modeling land surface processes in a general circulation model: 1. Model structure, Journal of Geophysical Research: Atmospheres, 105, 24809-24822, https://doi.org/10.1029/2000JD900327, 2000.

Kratzert, F., Klotz, D., Brenner, C., Schulz, K., and Herrnegger, M.: Rainfall–runoff modelling using long short-term memory (LSTM) networks, Hydrology and Earth System Sciences, 22, 6005-6022, https://doi.org/10.5194/hess-22-6005-2018, 2018.

Mane, S., Das, N., Singh, G., Cosh, M., and Dong, Y.: Advancements in dielectric soil moisture sensor Calibration: A comprehensive review of methods and techniques, Computers and Electronics in Agriculture, 218, 108686, https://doi.org/10.1016/j.compag.2024.108686, 2024.

https://doi.org/10.5194/egusphere-2026-3001
Preprint. Discussion started: 3 July 2026

Masters, D. and Luschi, C.: Revisiting small batch training for deep neural networks, arXiv preprint arXiv:1804.07612, https://doi.org/10.48550/arXiv.1804.07612, 2018.
Mittelbach, H., Lehner, I., and Seneviratne, S. I.: Comparison of four soil moisture sensor types under field conditions in Switzerland, Journal of Hydrology, 430, 39-49, https://doi.org/10.1016/j.jhydrol.2012.01.041, 2012.
Moon, H., Guillod, B. P., Gudmundsson, L., and Seneviratne, S. I.: Soil moisture effects on afternoon precipitation occurrence in current climate models, Geophysical research letters, 46, 1861-1869, https://doi.org/10.1029/2018GL080879, 2019.
Muñoz-Sabater, J., Dutra, E., Agustí-Panareda, A., Albergel, C., Arduini, G., Balsamo, G., Boussetta, S., Choulga, M., Harrigan, S., and Hersbach, H.: ERA5-Land: A state-of-the-art global reanalysis dataset for land applications, Earth system science data, 13, 4349-4383, https://doi.org/10.5194/essd-13-4349-2021, 2021.
Nair, V. and Hinton, G. E.: Rectified linear units improve restricted boltzmann machines, Proceedings of the 27th international conference on machine learning (ICML-10), 807-814,
Novick, K. A., Biederman, J., Desai, A., Litvak, M., Moore, D. J., Scott, R., and Torn, M.: The AmeriFlux network: A coalition of the willing, Agricultural and Forest Meteorology, 249, 444-456, https://doi.org/10.1016/j.agrformet.2017.10.009, 2018.
O, S. and Orth, R.: Global soil moisture data derived through machine learning trained with in-situ measurements, Scientific Data, 8, 170, https://doi.org/10.1038/s41597-021-00964-1, 2021.
Ojo, E. R., Bullock, P. R., L'Heureux, J., Powers, J., McNairn, H., and Pacheco, A.: Calibration and evaluation of a frequency domain reflectometry sensor for real-time soil moisture monitoring, Vadose Zone Journal, 14, vzj2014. 2008.0114, https://doi.org/10.2136/vzj2014.08.0114, 2015.
Pastorello, G., Trotta, C., Canfora, E., Chu, H., Christianson, D., Cheah, Y.-W., Poindexter, C., Chen, J., Elbashandy, A., and Humphrey, M.: The FLUXNET2015 dataset and the ONEFlux processing pipeline for eddy covariance data, Scientific data, 7, 1-27, https://doi.org/10.1038/s41597-020-0534-3, 2020.
Richards, J. H. and Caldwell, M. M.: Hydraulic lift: substantial nocturnal water transport between soil layers by Artemisia tridentata roots, Oecologia, 73, 486-489, https://doi.org/10.1007/BF00379405, 1987.
Santanello, J. A., Dirmeyer, P. A., Ferguson, C. R., Findell, K. L., Tawfik, A. B., Berg, A., Ek, M., Gentine, P., Guillod, B. P., and Van Heerwaarden, C.: Land–atmosphere interactions: The LoCo perspective, Bulletin of the American Meteorological Society, 99, 1253-1272, https://doi.org/10.1175/BAMS-D-17-0001.1, 2018.
Seneviratne, S. I., Corti, T., Davin, E. L., Hirschi, M., Jaeger, E. B., Lehner, I., Orlowsky, B., and Teuling, A. J.: Investigating soil moisture–climate interactions in a changing climate: A review, Earth-Science Reviews, 99, 125-161, https://doi.org/10.1016/j.earscirev.2010.02.004, 2010.
Seo, E. and Dirmeyer, P. A.: Understanding the diurnal cycle of land–atmosphere interactions from flux site observations, Hydrology and Earth System Sciences, 26, 5411-5429, https://doi.org/10.5194/hess-26-5411-2022, 2022.
Seo, E., Dirmeyer, P. A., Barlage, M., Wei, H., and Ek, M.: Evaluation of Land–Atmosphere Coupling Processes and Climatological Bias in the UFS Global Coupled Model, Journal of Hydrometeorology, 25, 161-175, https://doi.org/10.1175/JHM-D-23-0097.1, 2024.
Seo, E., Lee, M.-I., Schubert, S. D., Koster, R. D., and Kang, H.-S.: Investigation of the 2016 Eurasia heat wave as an event of the recent warming, Environmental Research Letters, 15, 114018, https://doi.org/10.1088/1748-9326/abbbae, 2020.
Seo, E., Lee, M.-I., Jeong, J.-H., Koster, R. D., Schubert, S. D., Kim, H.-M., Kim, D., Kang, H.-S., Kim, H.-K., and MacLachlan, C.: Impact of soil moisture initialization on boreal summer subseasonal forecasts: mid-latitude surface air temperature and heat wave events, Climate Dynamics, 52, 1695-1709, https://doi.org/10.1007/s00382-018-4221-4, 2019.
Simonyan, K., Vedaldi, A., and Zisserman, A.: Deep inside convolutional networks: Visualising image classification models and saliency maps, arXiv preprint arXiv:1312.6034, https://doi.org/10.48550/arXiv.1312.6034, 2013.
Srivastava, N., Hinton, G., Krizhevsky, A., Sutskever, I., and Salakhutdinov, R.: Dropout: a simple way to prevent neural networks from overfitting, The journal of machine learning research, 15, 1929-1958, 2014.
Sun, J., Yang, K., He, X., Wang, G., Wang, Y., Yu, Y., and Lu, H.: Causal pathways underlying global soil moisture–precipitation coupling, Nature Communications, 16, 8935, https://doi.org/10.1038/s41467-025-63999-7, 2025.
Tak, S., Seo, E., Dirmeyer, P. A., and Lee, M.-I.: The role of soil moisture-temperature coupling for the 2018 Northern European heatwave in a subseasonal forecast, Weather and Climate Extremes, 100670, https://doi.org/10.1016/j.wace.2024.100670, 2024.
Taylor, C. M., de Jeu, R. A., Guichard, F., Harris, P. P., and Dorigo, W. A.: Afternoon rain more likely over drier soils, Nature, 489, 423-426, https://doi.org/10.1038/nature11377, 2012.
Wang, Y., Shi, L., Hu, Y., Hu, X., Song, W., and Wang, L.: A comprehensive study of deep learning for soil moisture prediction, Hydrology and Earth System Sciences, 28, 917–943, https://doi.org/10.5194/hess-28-917-2024, 2024.
Wei, J. and Dirmeyer, P. A.: Dissecting soil moisture-precipitation coupling, Geophysical Research Letters, 39, https://doi.org/10.1029/2012GL053038, 2012.
Zreda, M., Shuttleworth, W., Zeng, X., Zweck, C., Desilets, D., Franz, T., and Rosolem, R.: COSMOS: The cosmic-ray soil moisture observing system, Hydrology and Earth System Sciences, 16, 4079-4099, https://doi.org/10.5194/hess-16-4079-2012, 2012.

https://doi.org/10.5194/egusphere-2026-3001
Preprint. Discussion started: 3 July 2026

Figure

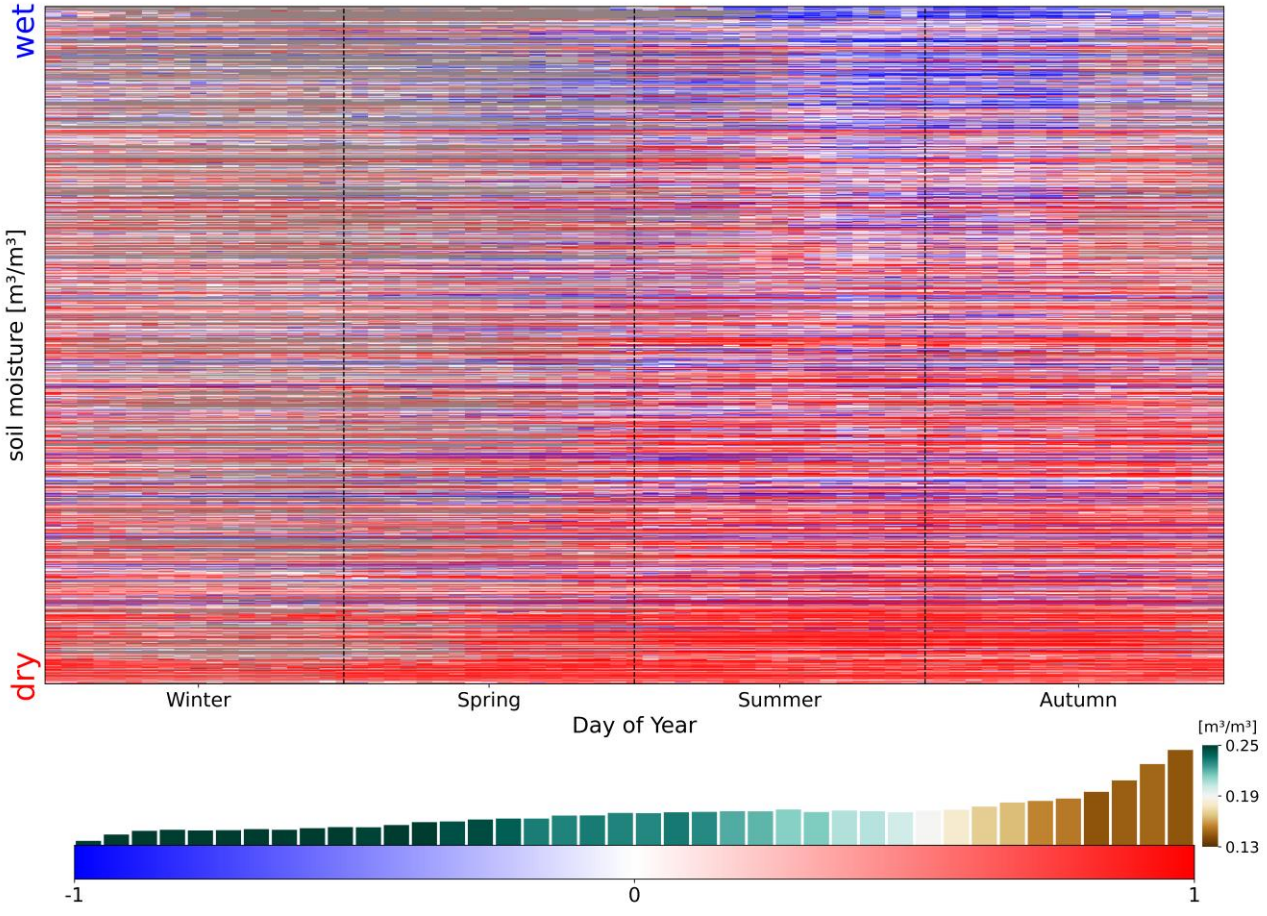

595 **Figure 1: Heatmap of temporal correlation coefficients between diurnal surface SM and TS cycles across in-situ measurement sites. The y-axis represents individual sites, sorted from top (wettest) to bottom (driest) based on their SM climatology. The x-axis denotes the day of year with 5-day window, where each grid cell represents the multi-year average of the correlation calculated for 24-hour diurnal cycles. The grey area indicates periods for which the diurnal correlation cannot be calculated because a complete 24-hour SM time series is unavailable for a given calendar date across multiple observation years. Histogram above the horizontal**
600 **color bar illustrates the frequency distribution of these temporal correlations, with the bar colors indicating the mean SM climatology for each correlation bin, as defined by the vertical color scale on the right.**

https://doi.org/10.5194/egusphere-2026-3001
Preprint. Discussion started: 3 July 2026

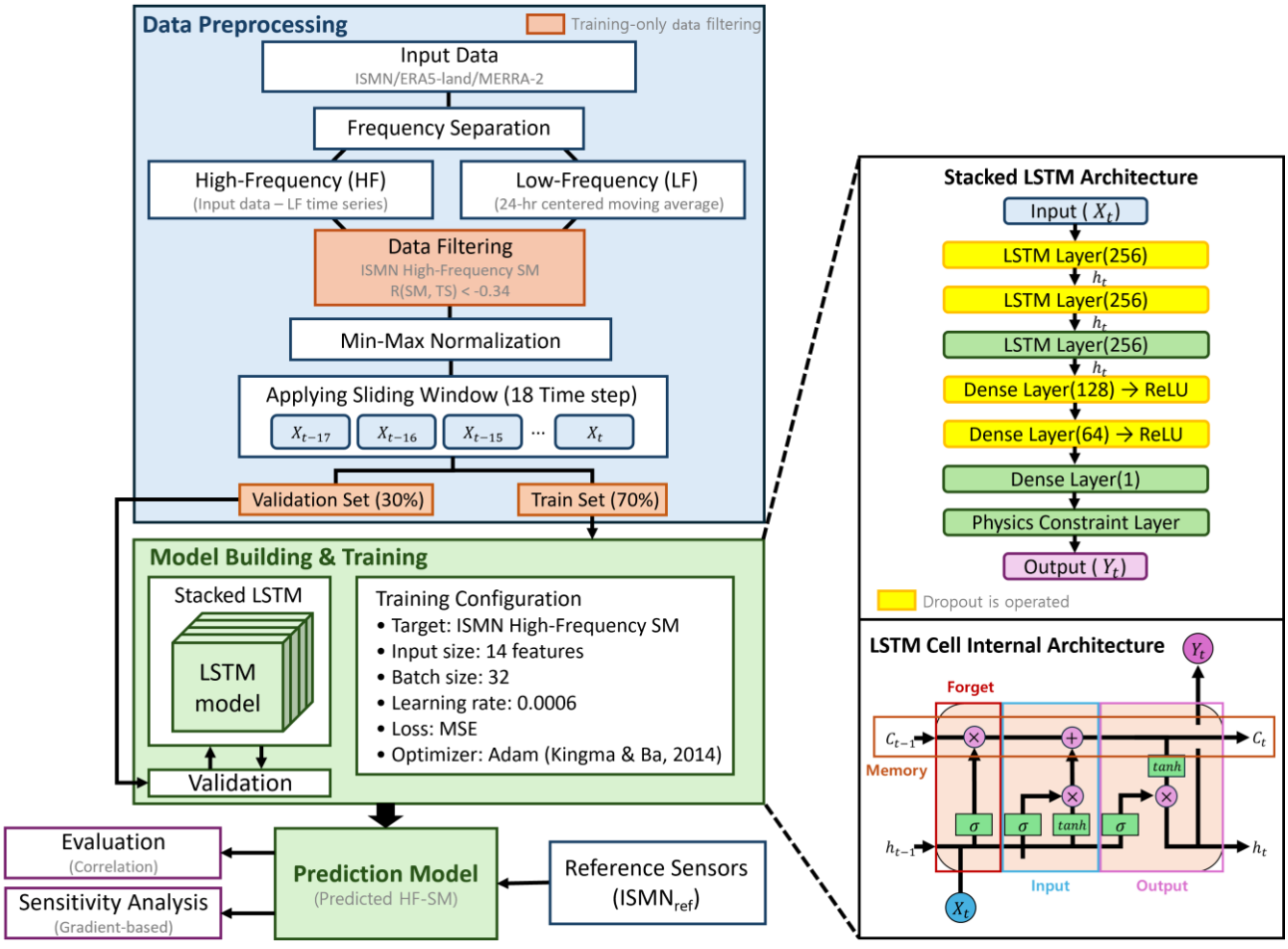

Figure 2: Schematic workflow of the LSTM modeling process for correcting SM time series.

https://doi.org/10.5194/egusphere-2026-3001
Preprint. Discussion started: 3 July 2026

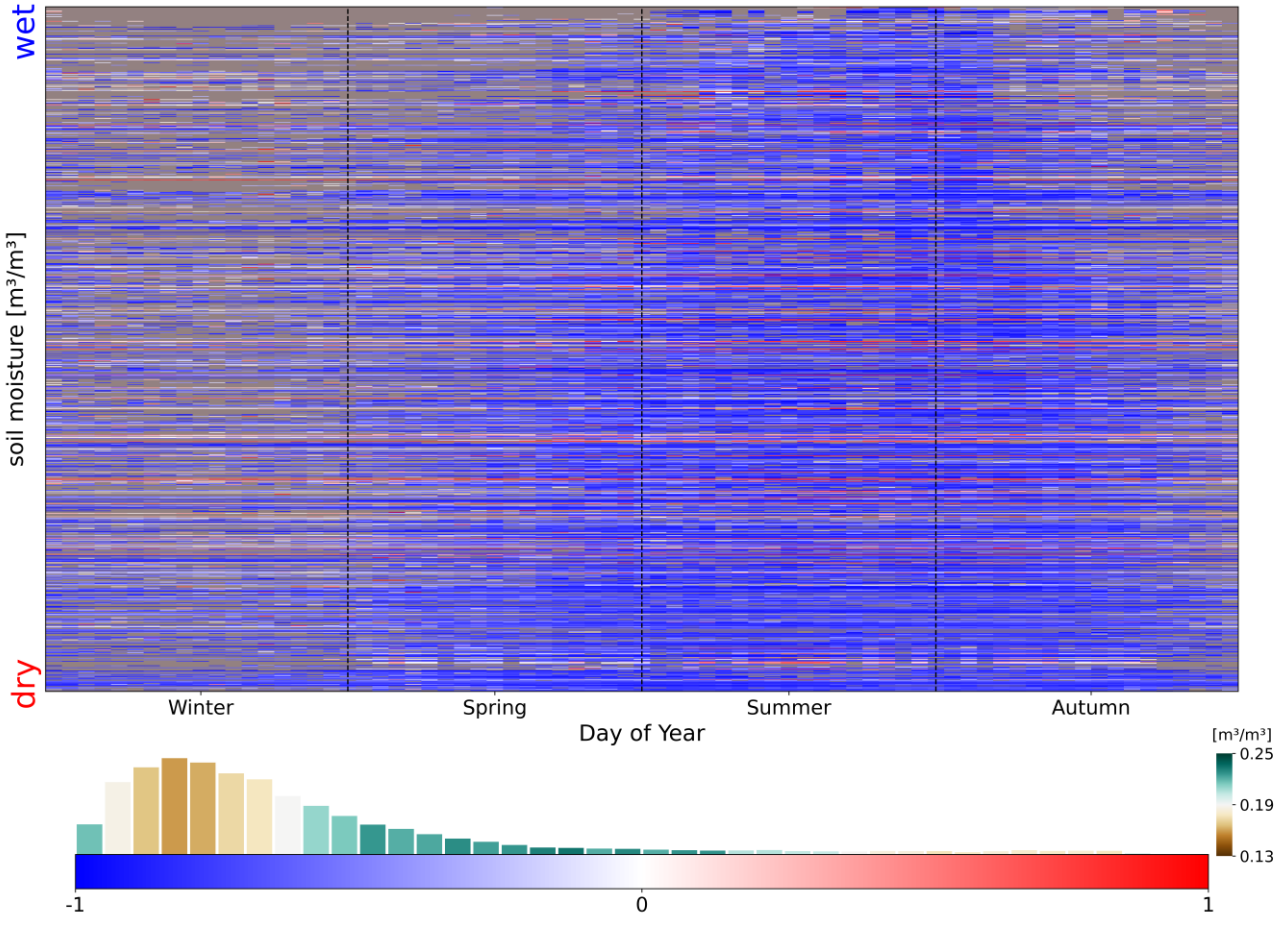

605 **Figure 3: Same as Fig. 1, but for using SM observations temporally corrected via a LSTM-based approach.**

https://doi.org/10.5194/egusphere-2026-3001
Preprint. Discussion started: 3 July 2026

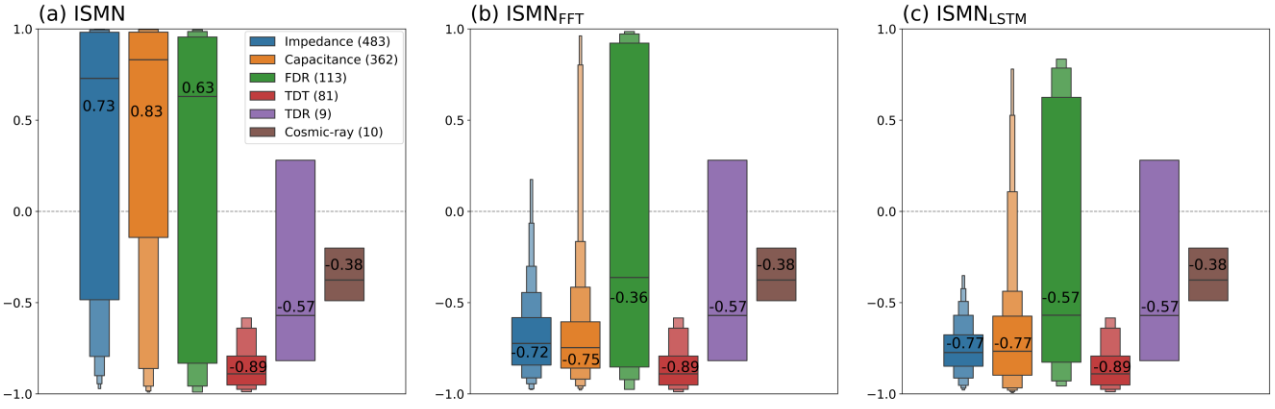

Figure 4: Boxplot of the temporal correlation of hourly time series between surface TS and SM from (a) ISMN (same as Fig. 2a of Han et al., 2026), (b) ISMN$_{FFT}$, and (c) ISMN$_{LSTM}$, across six different measurement sensor types, where median values are denoted beside each boxplot. Values in parentheses in the legend represent (a) the number of stations using each sensor type.

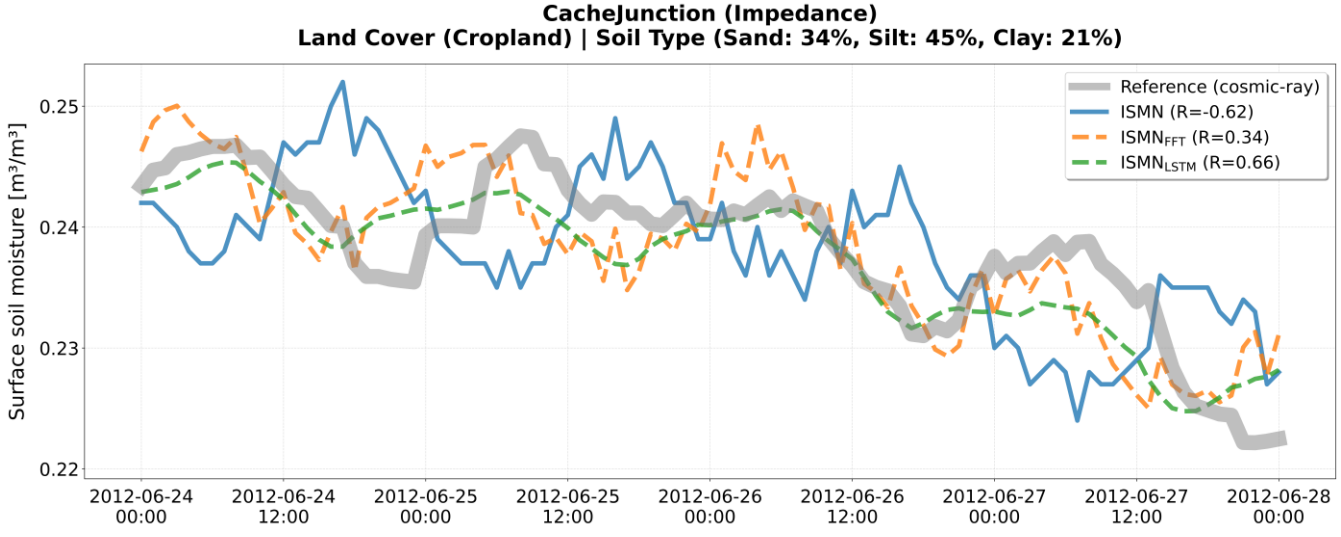

Figure 5: Hourly time series of surface SM at Cache Junction SCAN site (41.49°N, 111.59°W) from June 24 to June 28, 2012. The gray line indicates the reference cosmic-ray observations from the T.W. Daniel Experimental Forest (TWDEF) COSMOS site (41.86°N, 111.5°W). The blue, orange dashed, and green dashed lines represent the original ISMN, ISMN$_{FFT}$, and ISMN$_{LSTM}$ time series, respectively. The temporal correlation coefficient between the ISMN-based products and reference is noted in the legend.

https://doi.org/10.5194/egusphere-2026-3001
Preprint. Discussion started: 3 July 2026

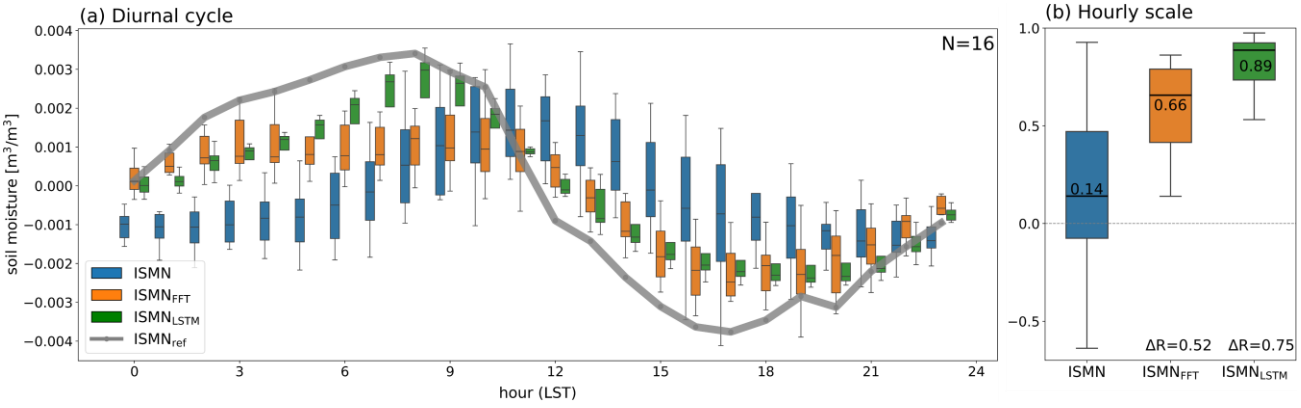

Figure 6: (a) Composite diurnal cycle of surface SM anomaly aggregated across 16 in-situ measurement sites from electrical-based ISMN (blue), ISMN$_{FFT}$ (orange), ISMN$_{LSTM}$ (green), and reference sensors (gray line). To compare the impact of diurnal adjustment on electric-based measurements with the reference sensors, the 16 closest electric-based observations are sampled within 50 km from the reference sensors. (b) Distribution of hourly-scale temporal correlation coefficients between the diurnal SM time series of ISMN (blue), ISMN$_{FFT}$ (orange), and ISMN$_{LSTM}$ (green) against the corresponding reference observations.

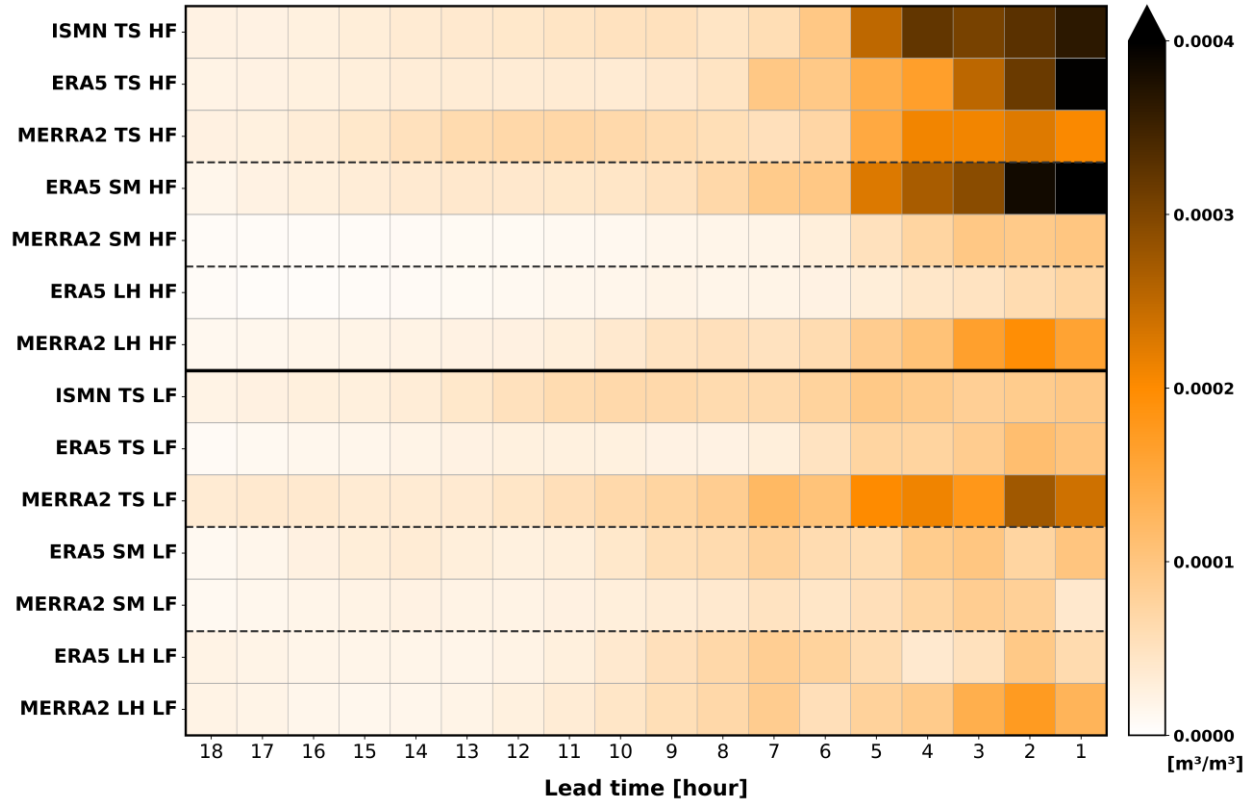

Figure 7: Heatmap of gradient-based lag-dependent sensitivity for LSTM input variables (y-axis) across different lead times (x-axis). The color represents the magnitude of the sensitivity, illustrating the temporal evolution of relative importance for SM prediction.

https://doi.org/10.5194/egusphere-2026-3001
Preprint. Discussion started: 3 July 2026

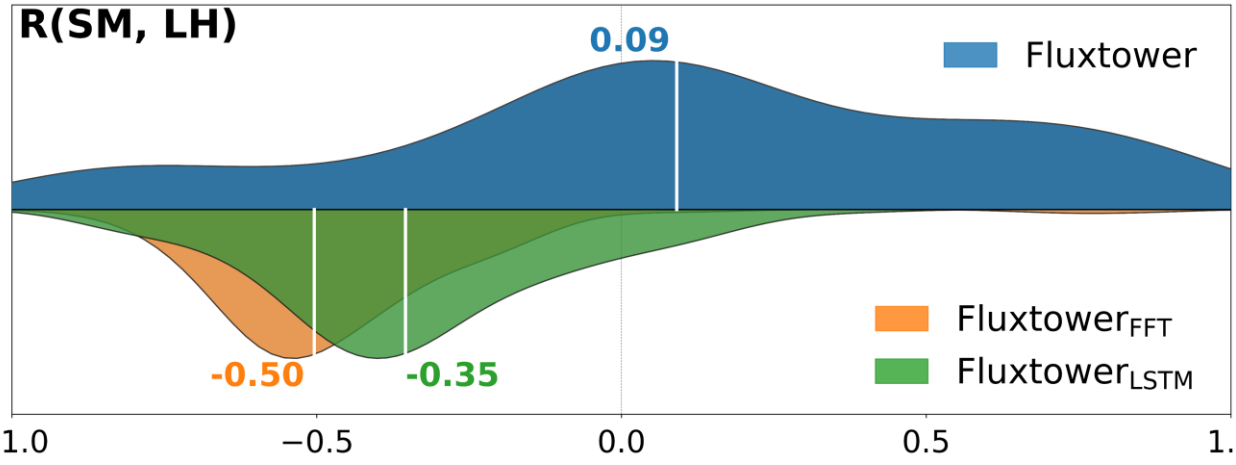

Figure 8: Violin plots of the correlation coefficient between SM and LH derived from the original flux tower observations (Fluxtower, blue), Fourier-transform-based diurnally adjusted observations (Fluxtower$_{FFT}$, orange; Han et al., 2026), and LSTM-based adjusted observations (Fluxtower$_{LSTM}$, green) across N=178 sites at the hourly timescale during the hemispheric warm season (MJJAS for the Northern Hemisphere and NDJFM for the Southern Hemisphere). Median values are indicated by vertical white lines.